Title: Modulating behavioral signatures of rhythmic auditory entrainment with tACS

Abbreviated title: tACS effects on rhythmic auditory perception

Authors: Yuranny Cabral-Calderin[1]*, Daniela van Hinsberg[1], Axel Thielscher[2,3] & Molly J. Henry[1,4]*

Affiliations: [1]Max Planck Institute for Empirical Aesthetics, 60322, Frankfurt am Main, Germany. [2]Danish Research Centre for Magnetic Resonance, Centre for Functional and Diagnostic Imaging and Research, Copenhagen University Hospital Amager and Hvidovre, Denmark. [3]Section for Magnetic Resonance, DTU Health Tech, Technical University of Denmark, Kgs Lyngby, Denmark. [4]Toronto Metropolitan University, Toronto, Canada.

*** Corresponding author email address:**

yuranny.cabral-calderin@ae.mpg.de

molly.henry@ae.mpg.de

Conflict of Interest Statement: The authors declare no competing interest.

Acknowledgments: This work was supported by a European Research Council Starting Grant (BRAINSYNC) and a Max Planck Research Group granted to MJH. AT was supported by the Lundbeck foundation (grants R244-2017-196 and R313-2019-622). We thank Hanna Kadel, Dominik Thiele, and Cornelius Abel for technical support. We thank the MRI core Unit of the Brain Imaging Center in Frankfurt for technical support setting up the MRI sequences.

Abstract

Synchronization between auditory stimuli and brain rhythms is beneficial for processing auditory information. In principle, auditory perception could be improved by facilitating neural entrainment to sounds via brain stimulation. Here we aimed to modulate auditory perception by modulating neural entrainment to frequency modulated (FM) sounds using transcranial alternating current stimulation (tACS). In addition, we aimed to evaluate the advantage of using tACS montages spatially optimized for each individual's anatomy and functional data compared to a standard montage applied to all participants. Across two different sessions, 2-Hz tACS was applied targeting auditory brain regions either with a standard or with an individually optimized electrode montage. Concurrent with tACS, participants listened to FM stimuli with modulation rate matching the tACS frequency but with different phase lags relative to the tACS, and detected silent gaps embedded in the FM sound. As expected, gap detection was sinusoidally modulated by the phase of the 2-Hz FM stimulus into which the gap fell. TACS did not affect the optimal FM-stimulus phase for gap detection, but it modulated the amplitude of the FM-stimulus induced behavioral modulation – a behavioral signature of the strength of neural entrainment – in a phase-lag specific manner. Both the optimal tACS lag and the magnitude of the tACS effect were variable across participants and sessions. Inter-individual variability of tACS effects was explained by the interactions between different electric field properties including the strength of the inward electric field, the field focality and the proximity of the electric field peak to the target brain region. Although no main effect of tACS montage was observed on the strength of tACS effects, our results suggest lower inter-individual variability in the individualized-montage group compared to the standard group. Taken together, our results show that tACS is an effective tool to modulate behavioral entrainment to sounds, and its efficacy depends on the specific properties of the applied electric field. However, the lack of reliability on optimal tACS lags calls for caution when planning tACS experiments based on separate sessions.

Significance Statement

Neural activity synchronizes to the rhythms in sounds via neural entrainment, which seems to be important for successful auditory perception. A natural hypothesis is that improving neural entrainment, for example via brain stimulation, should benefit perception. Here we applied transcranial electrical stimulation with alternating currents to modulate the strength with which brain activity entrains to rhythmic auditory stimuli and affects behavior. We observed that the electrical stimulation affected the strength with which the auditory stimulus modulated the detection of near-threshold target events depending on the lag between the sound and the electrical signal. Inter-individual variability in the observed effects could be explained by the strength and focality of the simulated electric field depending on how close was the electric field to the relevant brain region.

Introduction

Brain rhythms synchronize with – entrain to – rhythms in sounds, and this stimulus-brain synchrony potentially facilitates perception and comprehension of auditory sensory information [1-8]. For example, successful neural entrainment seems to support cocktail-party listening – in a cocktail party scenario, speech tracking in and near low-level auditory cortices is enhanced for attended vs. ignored speech, and only attended speech has been observed to be tracked in higher-order brain regions [2]. In addition, stronger neural entrainment to the beat in music has been associated with superior beat prediction abilities and with better movement synchronization accuracy with a rhythmic beat [7]. Thus, stronger neural entrainment to auditory rhythms seems to support successful and adaptive listening.

If entrainment to auditory rhythms is really beneficial for auditory perception, then improving entrainment via external manipulations should lead to corresponding improvements in auditory perception. One technique often used to interfere with neural entrainment is transcranial alternating current stimulation (tACS). During tACS, a low-intensity alternating current is applied to scalp electrodes with the aim of reaching the brain and entraining brain activity to the electrical stimulation [9-11]. The efficacy of tACS-entrainment has been supported by studies showing increased power in EEG signals at the frequency of the electrical stimulation as well as phase alignment of intrinsic brain activity to the applied alternating current in single-unit recordings [12,13].

In the auditory domain, tACS has been shown to significantly modulate speech comprehension, stream segregation, and binaural integration [14-20]. For example, 4-Hz tACS modulates segregation of an auditory stream from background in a cyclic manner [14]. In addition, tACS synchronized with the speech envelope of attended as well as ignored speech signals in a cocktail-party scenario modulates speech comprehension of the target speech, albeit with opposite phase relationship [21].

Despite the promising findings, inconsistent results across studies have led to questions regarding the robustness, reliability, and reproducibility of tACS effects [22,23]. Intra-individual reliability of tACS effects is often overlooked since multi-session tACS studies, where the same tACS protocol is repeatedly tested, are scarce. In addition, tACS effects have been shown to be state-dependent and variable across participants [24,25]. Inter-

individual variability on tACS effects might also arise from variability in brain anatomy, leading to inter-individual variability in the electric field induced by tACS when using the same electrodes montage and current strength [26]. Indeed, inter-individual variability in electric field strength predicts inter- individual variability in tACS effects [24,27,28]. Thus, using the same tACS parameters (frequency, current strength, electrode position) might not be optimal for every participant or for a given participant under different conditions. Rather, optimal tACS protocols might need to be tailored to each participant to target the right frequency [29] or stimulus-brain lag [18] in the relevant brain region. Yet, studies testing the benefits of individually optimized tACS montages are scarce in the field.

In the present study, we test 1) the efficacy of tACS for modulating auditory perception, 2) the benefits of using individually optimized tACS montages for modulating behavior, and 3) the within-participant reliability of tACS results. Across two different sessions, participants listened to a frequency modulated (FM) noise stimulus and detected silent gaps presented at different phase positions within an FM cycle, while tACS was applied at different phase lags relative to the FM stimulus. Using structural and functional magnetic resonance imaging (fMRI), we optimized the tACS montage to target individually defined functional targets and tested its superiority over a group montage both in terms of the induced electric fields and the magnitude and variability of tACS effects on performance. Specifically, we ask 4 questions: 1) can tACS at different phase lags interfere with stimulus-brain synchrony and modulate the behavioral signatures of entrainment? 2) are tACS effects reliable over time? 3) what factors predict individual variability of tACS effects? And 4) do tACS montages individually optimized in terms of spatial location yield stronger modulations of auditory perception?

Results

Using fMRI and FEM models to individually optimize tACS montages

Using one-size-fits-all montages for tACS can lead to high inter-individual variability in terms of the induced electric field and the strength of tACS effects. Here, we go a step past the current literature by individualizing the tACS montages to target individually defined functional targets and compare their performance relative to two

118 different group montages previously used in the literature for targeting auditory regions
119 [18,30].

120 Listeners participated in one magnetic resonance imaging (MRI) session where
121 functional and structural MRI datasets were collected. During the functional runs,
122 participants listened to a 2-Hz FM stimulus and detected silent gaps presented at different
123 phase locations along the modulation cycle (**Fig. 1a,** see Methods). As expected, increased
124 BOLD signal in auditory temporal areas, including bilateral Heschl's gyri and superior
125 temporal gyrus, was observed in response to the auditory stimulus (**Fig. 1b**). Target regions
126 of interest (ROI) were defined for each individual as the brain regions exhibiting the
127 strongest response to the FM-stimulus (one per hemisphere, see Methods, **Fig. 1c, e, Table**
128 **S1**).

129 Using individual finite element method (FEM) head models (see Methods), the
130 individual electrode montage was optimized in SimNIBS to focus the electric field as
131 precisely as possible at the target ROI with a field orientation matching an auditory dipole
132 as estimated in a previous study targeting auditory regions [30], and a desired field intensity
133 of 0.09 V/m (**Fig. 1d-g**, see Methods). The resulting individual montages varied across
134 participants and could take on two out of seven different electrode positions for the left
135 hemisphere: FC5, C1, C3, C5, T7, TP7, P7, and two out of nine different electrode
136 positions for the right hemisphere: FC4, FC6, C2, C4, C6, T8, TP8, P8 and PO8. Despite
137 some variability, the most common montages included the electrodes C5-TP7 and C6-TP8,
138 with for example TP7 being used for 34 out of 39 participants (**Fig. 1f**).

139 Electric field simulations were performed for each individual brain using the
140 individually optimized montage (from now on referred to as *individualized montage*) with
141 electrodes placed differently across participants, as well as two additional montages from
142 the literature, with electrodes placed at the same positions across participants (**Fig. 2a,** see
143 Methods): 1) same electrode shape and size as for the *individualized montage* but placed
144 over FC5-TP7/P7 and FC6-TP8/P8 (referred to as *standard montage* in the rest of the

document) as in [30], and a high-definition montage (*HD-montage*) with center electrodes placed over T7 and T8 similar to the montage previously used by [18].

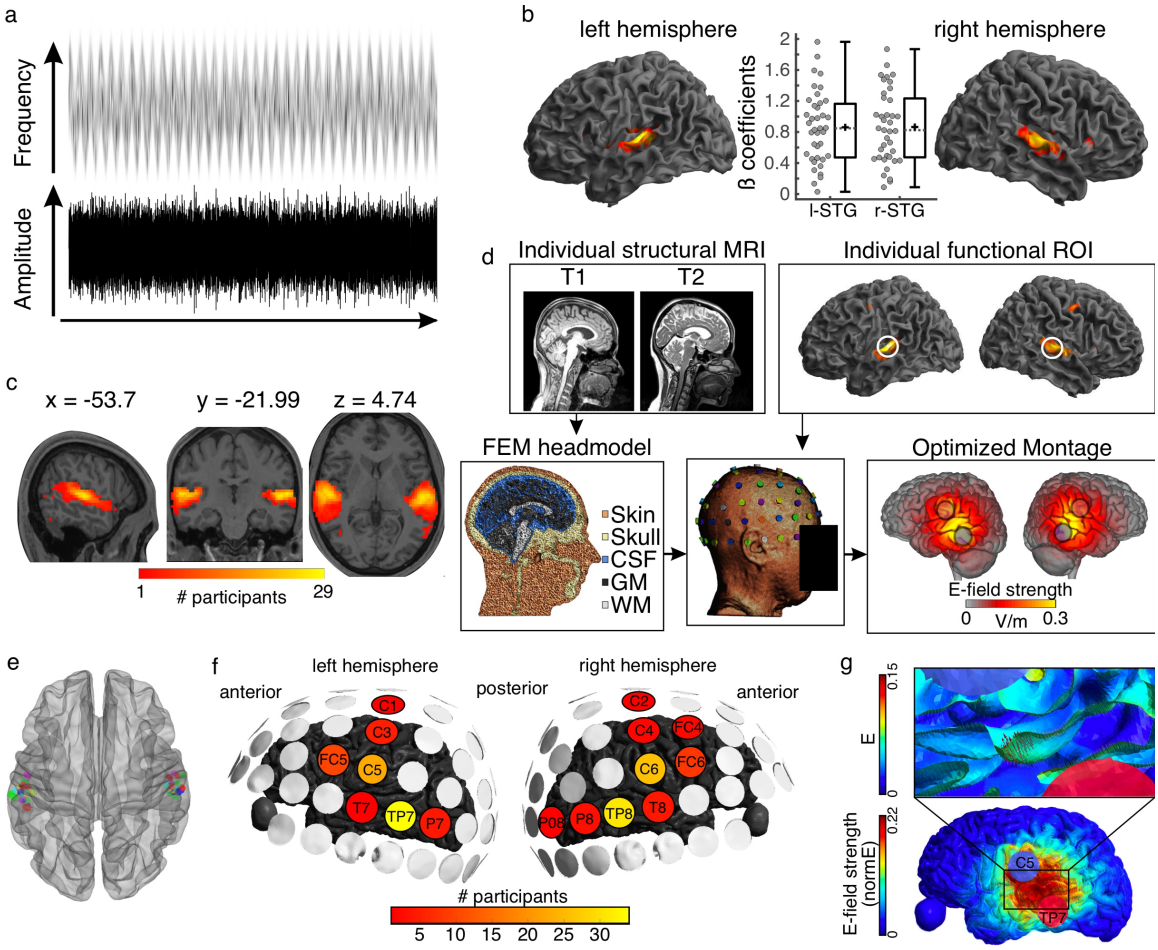

Figure 1. Auditory stimulus and tACS optimization pipeline. a) Stimulus representation. A complex noise stimulus is frequency modulated at 2 Hz without any rhythmic modulation of its amplitude. Silent gaps are presented at different phase locations of the FM-stimulus modulation cycle. **b)** Group data showing the regions exhibiting higher BOLD signal during the FM-stimulus presentation compared to the implicit baseline, p(FWE) < 0.05. Distribution plots in the center show the beta estimates extracted for the whole cluster for each participant per hemisphere. Box plots show median (horizontal dashed lines), mean (black cross), 25th and 75th percentiles (box edges) and extreme datapoints not considered outliers (+/– 2.7σ and 99.3 percentiles, whiskers). Each circle represents a single participant. **c)** Overlap of single-participant binary masks after thresholding the individual t-maps for the same contrast as shown in **(b). d)** Pipeline for optimizing the tACS electrode montage for each individual participant to target the individual functional targets. **e)** Target regions of interest used for the optimization step in SimNIBS. Individual dots represent the individual 3-mm-radius spheres around the center coordinates from the functional masks shown in **(c). f)** Electrodes included in the optimized montages across participants. **g)** Electric field (E) and electric field strength (normE) resulting from the optimized montage for one example participant.

Only the left hemisphere is shown. Blue and red circles denote the resulting electrodes. Small red arrows on the inset show the target E-field orientation.

To compare between tACS montages in terms of their simulated electric field profiles, seven different dependent measures were computed for each participant and montage. Two measures referred to spatial targeting: 1) mean Euclidian distance between the center coordinates of the functional ROIs (one per hemisphere) and the center coordinates of the peak of the electric field in each hemisphere (where the peak is for the 99-percentile-thresholded E-field strength across all voxels for the given hemisphere) and 2) spatial Pearson correlation coefficient between the individual BOLD signal t-map and the electric field map. Four measures quantified the electric field (E-field) strength: 3) peak E-field strength for the whole brain (based on the 95-percentile-thresholded E-field map), 4) mean peak E-field strength in the functional ROIs (based on the 95-percentile-thresholded E-field from a 7 mm sphere around the center coordinates of the functional ROIs), 5) peak normal component of the E-field for the whole brain (95-percentile-thresholded), and 6) peak normal component of the E-field in the functional ROI (defined as in 4). The last measure quantified 7) E-field focality (cortical area in mm² with E-field strength higher than the 50th percentile). Repeated measures analysis of variance (rmANOVA) showed a significant effect of montage on all of the investigated measures (all $F_{(2,76)} \geq 9.938$, $p \leq 1.5e\text{-}04$, **Fig. 2b**).

Regarding the spatial targeting of the functional ROI, the Euclidian distance between the E-field peaks and the target functional ROIs averaged across hemispheres was higher for the HD-montage compared to both the individualized and the standard montages (all $t_{(38)} \geq 4.986$, $p \leq 4.163e\text{-}05$, *Bonferroni corrected*). Fisher-Z-transformed correlation values between the E-field map and the BOLD signal map were also higher for the HD-montage compared to both individualized and standard montages (all $t_{(38)} \geq 2.798$, $p \leq 0.024$, *Bonferroni corrected*). Thus, the HD-montage produced electric fields that were better correlated with the functional activation maps across the entire brain than the other two montages, but peak electric field missed the mark. No significant difference between the standard and the individualized montage was observed either for the distance between

the E-field and the functional map peaks or the E-field to BOLD correlation (all $|t|_{(38)} \leq 2.047$, $p \geq 0.143$, *Bonferroni corrected*).

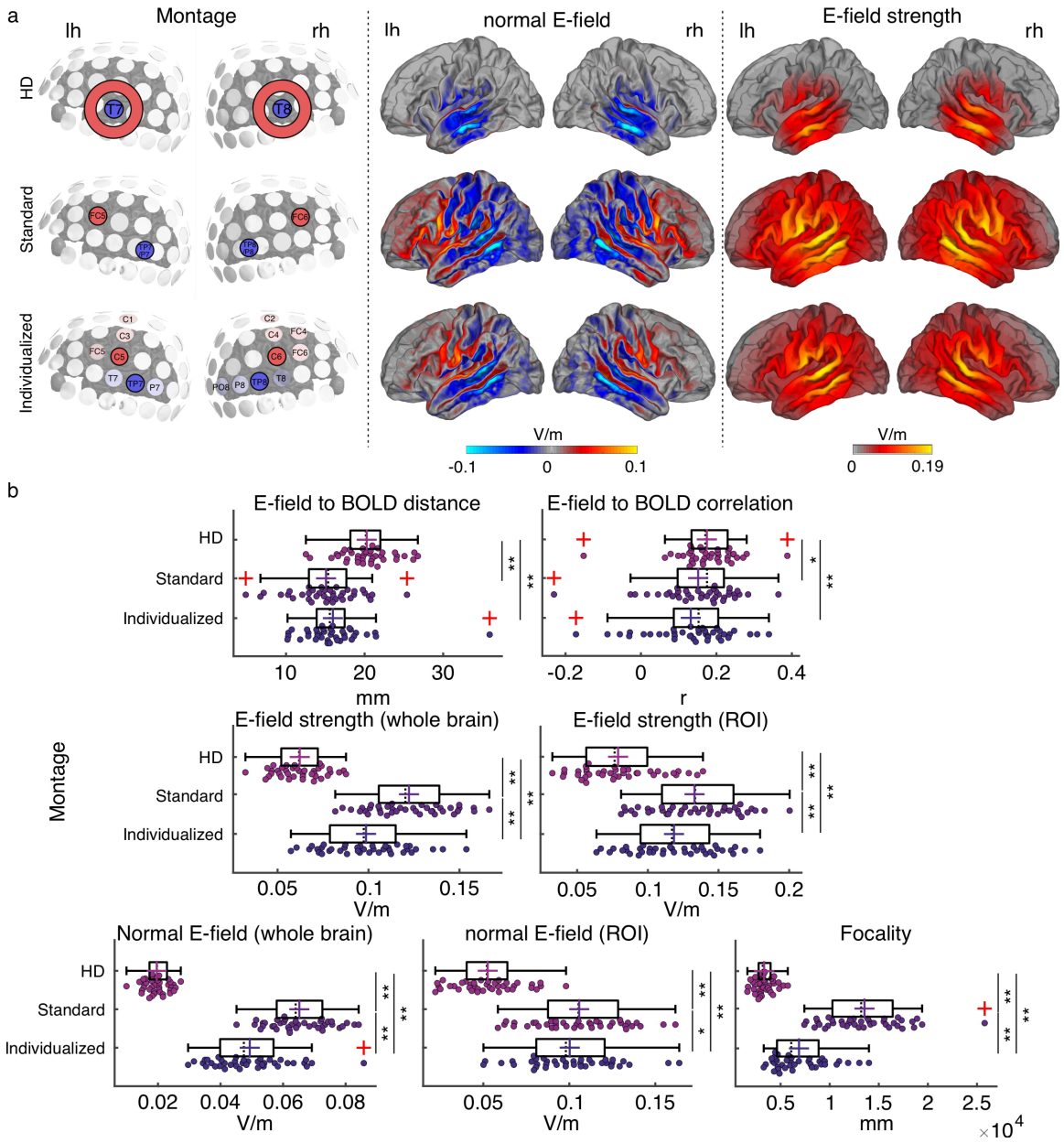

Figure 2. Electric field simulation results. a) Group average maps showing the strength of the simulated electric field (E-field strength, right) and its normal component (normal E-field, middle), separated by montage: high-definition montage (HD), top; standard montage, middle, and individualized montage, bottom. Each montage is represented in the left subpanel. **b)** Plots showing the individual values for the seven E-field parameters estimated per montage and participant. Each dot represents a single participant. Box plots show median (dashed vertical lines), mean (cross in the middle of the box), 25th and 75th percentiles (box edges) and extreme datapoints not considered outliers (+/–2.7σ and 99.3 percentiles,

whiskers). Red crosses represent outliers (more than 1.5 times the interquartile range away from the bottom or top of the box). Note that outliers were not excluded from analyses. *p < 0.05, **p < 0.001, Bonferroni corrected.

Regarding E-field strength, the standard montage induced higher electric field than the HD and the individualized montages for the whole brain and within the ROI; the same was true when considering only its normal component (all $t_{(38)} \geq 2.568$, $p \leq 0.043$, *Bonferroni corrected,* **Fig. 2b**). The individualized montage showed stronger E-field and normal component of the E-field, for the whole brain and within the ROI, when compared to the HD-montage (all $t_{(38)} \geq 13.43$, $p \leq 1.665e\text{-}15$, *Bonferroni corrected,* **Fig. 2b**). In terms of focality, the HD-montage was the most focal of the three (all $t_{(38)} \geq 8{,}098$, $p \leq 2.54e\text{-}9$, *Bonferroni corrected,* **Fig. 2b**), followed by the individualized montage which was more focal than the standard ($t_{(38)} = 9.578$, $p = 3.349e\text{-}11$, *Bonferroni corrected,* **Fig. 2b**). Thus, each montage has its pros and cons, and the choice of montage will depend on which of these dependent measures is prioritized. The critical question then is which measure – or combination of measures – best predicts inter-individual variability in the magnitude of the tACS effect on behavior.

Before running any simulations, we had decided a priori to use only the individualized and standard montages for our main behavioral experiment (see below), motivated by the fact that the 4-electrode arrangement allows for directing the E-field in a desired orientation [30]. Targeting a specific field orientation would not be possible using the ring-electrode configuration from the HD montage. In addition, comparing between the simulated E-fields across montages showed that the HD-montage might in fact not be optimal for modulating oscillatory activity during our specific auditory task, since the peak of the induced E-field was farther away from our target ROI and its strength weaker compared to that simulated for the other two montages. As already described, we did not observe any difference between the individual and the group montages in terms of spatial overlap to our target ROI. While the electric field was strongest for the standard montage

compared to the individualized montage, the latter induced a more focal field compared to the standard montage, therefore each montage could be good in different ways.

FM-stimulus modulates gap detection with similar strength and optimal phase across participants and sessions

Across two different sessions, subjects listened to 2-Hz FM sounds and detected silent gaps presented at different phase locations on the FM modulation cycle. While performing the task, participants received either sham or verum tACS at 2 Hz (within participant) with either the individualized montage or the standard montage (between participants). During the verum tACS runs, the phase lag between the auditory stimulus and the tACS signal varied from trial to trial (**Fig. 3a**). Participants missing one session (N = 5) were excluded at this stage. All further analysis is presented for 37 participants (individualized montage: N=16, standard montage: N=21).

To evaluate the effect of the FM-stimulus phase on gap detection in the absence of tACS, gaps presented during the sham condition were binned according to the FM-stimulus phase into which the gap fell and the mean detection rate (hit rate) was computed for each bin (**Fig. 3b**). The strength of the FM-stimulus-driven behavioral modulation (*FM-amplitude*) and the optimal FM-stimulus phase (*FM-phase*) for gap detection were estimated by fitting a cosine function to hit rates as a function of FM-stimulus phase [31]. *FM-amplitude* was significantly higher than chance for 33/37 participants in session 1 and for 27/37 participants in session 2 (comparison between each participant's *FM-amplitude* and its corresponding surrogate distribution, $p < 0.05$, **Fig. 3c**). In addition, *FM-phase* was clustered across participants (Rayleigh test session 1: $Z = 29.031$, $p = 1.806e-17$; session 2: $Z = 26.531$, $p = 2.12e-15$). No significant difference between sessions was observed either for *FM-amplitude* ($t(36) = 0.99$, $p = 0.329$) or for *FM-phase* (inter session phase distance clustered around zero, $V = 28.391$, $p = 2.045e-11$). A significant correlation between sessions was observed for *FM-amplitude* (Pearson's $r = 0.516$, $p = 0.001$). The latter replicates our previous finding that the FM-stimulus driven modulation of gap detection performance is reliable across time. We retained the *FM-amplitude* and *FM-*

230 *phase* parameters as reliable signatures of behavioral entrainment to the FM-stimulus and

231 asked whether and how these signatures are modulated by tACS.

232

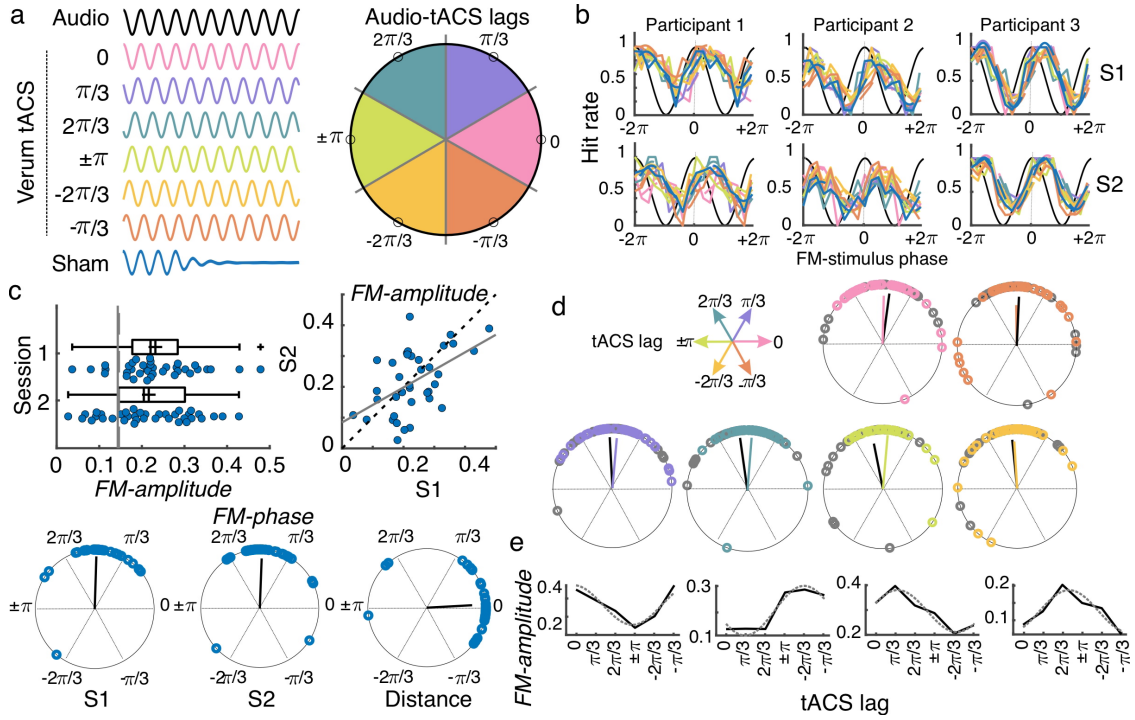

Figure 3. tACS effects and individual variability. a) While performing the auditory task, participants received either sham (blue) or 2-Hz tACS stimulation. The phase lag between the FM stimulus (black) and the tACS signal varied from trial to trial and was grouped into six different phase-lag bins. Each color in the figure represents a different bin. Empty black circles in the circular plot on the left mark the phase in the center of each bin. **b)** Hit rates as a function of FM-stimulus phase separated by tACS condition for both sessions (S1 and S2) from 3 example participants. Colors follow the same coding as in **(a). c)** Amplitude of the FM-stimulus driven behavioral modulation (FM-amplitude) and optimal FM-stimulus phase (FM-phase) in the sham condition. Left top plot shows the FM-amplitude values from the sham condition. Vertical lines represent the mean 95 percentile from individual surrogate distribution, session 1 dashed line, session 2 solid line. Each dot represents a single participant. Box plots show median (dashed vertical lines), mean (cross in the middle of the box), 25th and 75th percentiles (box edges) and extreme datapoints not considered outliers (+/–2.7σ and 99.3 percentiles, whiskers). Crosses represent outliers (more than 1.5 times the interquartile range away from the bottom or top of the box). Scatter plot on the right top shows the FM-amplitude in session 2 (S2) as a function of FM-amplitude in session 1 (S1). Dashed line is the diagonal and the solid line the best-fit regression line. Circular plots in the bottom panel show the optimal FM-phase for each session and the circular distance between sessions. The black line is the resultant vector. **d)** Optimal FM-phase separated by tACS lag condition. Each plot shows a different phase lag according to the coordinates presented in top left legend. Color code also matches that from panel **(a)**. For each plot, session 1 is presented in the corresponding color and session 2 in gray. The resultant vector is shown following the same convention. **e)** FM-amplitude as a function of tACS phase lag for 4 single-participant examples. Solid lines show true data and dashed lines the cosine fit. Only session one is shown.

tACS does not overwrite FM-stimulus driven behavioral entrainment

First, we tested a strong version of a hypothesis about how tACS would affect behavior, which is that tACS would "overwrite" neural entrainment to the FM stimulus. To do so, the phase lag between the FM-stimulus and tACS (Audio-tACS lag) was estimated for each trial. Gaps were grouped according to the FM-stimulus phase (9 bins) and the Audio-tACS lag (6 bins) and mean detection rates were computed for each FM-phase and Audio-tACS lag combination (**Fig. 3a-b**). A cosine function was fitted to the mean detection rates as a function of FM-stimulus phase, separated by Audio-tACS lag, and the amplitude and optimal phase parameters where estimated, similar to the sham condition. We hypothesized that tACS would interact with the FM-stimulus-driven neural entrainment and as such the behavioral signatures of entrainment – *FM-amplitude* and *FM-phase* – would vary as a function of Audio-tACS lag. First, if tACS overwrites entrainment to the FM-stimulus, we expect tACS phase to be more critical for gap detection than the phase of the auditory stimulus. As such, we anticipated a change in the FM-stimulus optimal phase as a function of Audio-tACS lag. Contrary to our expectations, in both sessions, optimal *FM-phase* was clustered across participants for all lag conditions around the same phase angle (V test with mean phase across lags as mean direction, all $V > 25.303$, $p < 2.016e\text{-}09$ **Fig. 3d**). The lack of tACS effect on *FM-phase* indicates that tACS does not overwrite neural entrainment to the FM stimulus.

tACS modulates the amplitude of the FM-stimulus driven behavioral entrainment

Our second hypothesis was that tACS could modulate the strength of entrainment to the FM stimulus, and as such, we expected *FM-amplitude* to be sinusoidally modulated by Audio-tACS lags: highest *FM-amplitude* should be observed for the optimal Audio-tACS lag since tACS would be aiding entrainment to the stimulus (constructive interference). In contrast, *FM-amplitude* was expected to be the smallest for tACS anti-phase to optimal lag: anti-phase tACS would disrupt entrainment to the FM stimulus since

260 the electrical signal and the auditory rhythms are working against each other (destructive
261 interference).

262 We wanted to test the effect of tACS lag on the FM-amplitude at the group level.
263 However, it is already known that the optimal tACS lag for auditory perception often shows
264 high inter-individual variability ([14], **Fig. 3e**), which can affect the estimation of group-level
265 tACS effects. To prevent inter-individual variability in optimal tACS lag from affecting
266 the estimation of tACS effects at the group level, 1) individual optimal tACS lag (*tACS-*
267 *phase*) was estimated for each participant and session using a cosine fit (Methods, ***Fig. 3e***)
268 and 2) tACS lags were realigned by making the optimal *tACS-phase* correspond to phase
269 zero and wrapping the remaining phases accordingly before doing group statistics (**Fig.**
270 **4a**). Data from the optimal tACS lag and its opposite lag (corresponding trough) were
271 excluded to avoid any artificial bias induced by the alignment procedure. Data from the
272 two tACS lags around the optimal lag were averaged and used as an estimate of the FM-
273 driven modulation in the optimal half of the tACS cycle (tACS(+)). Similarly, data from
274 the two tACS lags around the trough were averaged and used as an estimate of the FM-
275 driven modulation in the suboptimal half of the tACS cycle (tACS(-)). tACS effects were
276 tested using a repeated-measures ANOVA (rmANOVA) with the repeated measures tACS
277 lag condition (sham, tACS(+), tACS(-)) and session (1 and 2).

278 tACS did successfully modulate FM-stimulus driven behavioral entrainment (main
279 effect of tACS lag condition: $F_{(2, 144)} = 25.01$, $p < 0.001$, **Fig. 4b**). Post-hoc *t-tests* showed
280 that FM-driven modulation was higher for tACS(+) when compared to sham ($t(36) = 3.562$,
281 $p = 0.0032$ and to tACS(-) ($t(36) = 9.501$, $p < 0.001$, all p-values are *Bonferroni* corrected,
282 **Fig. 4b**). In addition, FM-driven modulation was significant lower at tACS(-) when
283 compared to sham ($t(36) = -3.090$, $p = 0.0115$, **Fig. 4b**). Neither the effect of session nor
284 the interaction of tACS lag x session were significant (Session $F_{(1,144)} = 0.03$, $p = 0.871$;
285 interaction tACS lag x session $F_{(2,144)} = 1.22$, $p = 0.298$). Thus, tACS modulated behavioral
286 signatures of neural entrainment to auditory rhythms, and critically both *amplified* and

attenuated entrainment relative to sham depending on the phase relationship between the electrical and auditory stimulation.

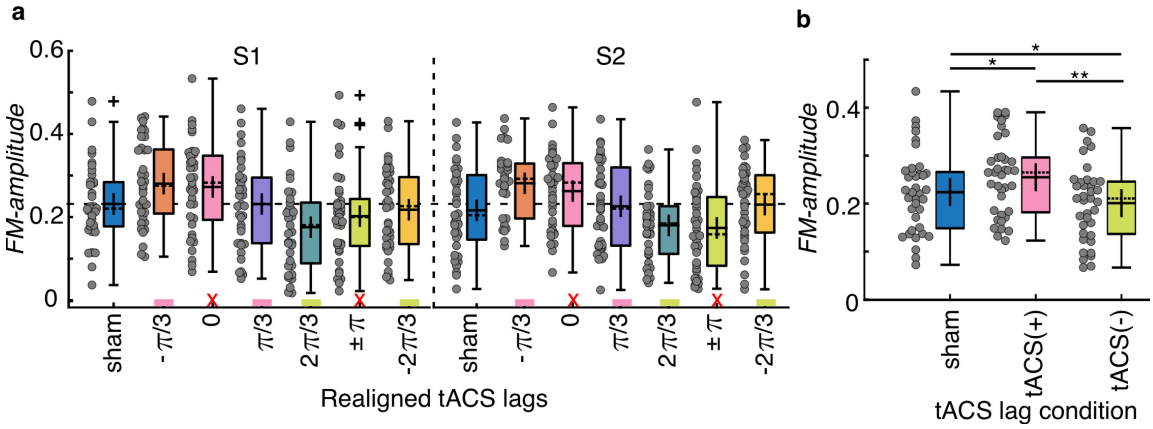

Fig 4. Group level tACS results. a) Amplitude of the FM-stimulus driven behavioral modulation (*FM-amplitude*) as a function of the realigned tACS lag conditions. Zero lag corresponds to each individual optimal tACS lag (based on a cosine fit). *FM-amplitude* for optimal lag and the opposite lag (marked with red x in the x-axis) were removed from further analyses and an estimate of *FM-amplitude* for the positive (tACS(+)) and negative tACS half cycles (tACS(-)) was obtained by averaging the individual FM-amplitude values from the two bins adjacent to the optimal lag (marked in pink in the x-axis) and its corresponding trough (marked in green in the x-axis), respectively. **b)** FM-amplitude values estimated for sham, tACS(+), and tACS(-), as described in **(a),** averaged over sessions. In all plots in the figure, each dot represents a single participant. Box plots show median (dashed vertical lines), mean (cross in the middle of the box), 25th and 75th percentiles (box edges) and extreme datapoints not considered outliers (+/–2.7σ and 99.3 percentiles, whiskers). Crosses represent outliers (more than 1.5 times the interquartile range away from the bottom or top of the box). S1: session 1, S2: session 2. *p = 0.05, **p < 0.001.

Inter-individual variability and reliability of tACS effects

So far, we have evaluated whether tACS at different phase lags interferes with stimulus-brain synchrony and modulates behavioral signatures of entrainment: *FM-amplitude* and *FM-phase*. At the group level, we observed no modulation of optimal FM-stimulus phase (*FM-phase*) but a significant effect of tACS-lag on the FM-stimulus driven behavioral modulation (*FM-amplitude*). Next, we asked how reliable tACS effects are over time both in terms of the strength of tACS effects and the optimal tACS lag. This is critical to quantify if we want to plan tACS interventions using data from different sessions. For example, if optimal tACS lag constitutes a stable individual trait measure, it could be

estimated in one session and used for applying tACS in following sessions to maximize treatment benefits.

To have a global measure of the magnitude of the tACS effect at the individual level, for each participant and session, the FM-driven modulation amplitude from the tACS negative half (tACS(-)) was subtracted from that during the tACS positive half (tACS(+)). This value was then interpreted as the amplitude of the tACS-induced behavioral modulation (*tACS-amplitude*, see Methods, **Fig. 5a**). To evaluate the reliability of the tACS induced modulation, *tACS-amplitude* values were compared and correlated between sessions. While no significant difference was observed between sessions, *tACS-amplitude* estimates did not correlate between sessions (session 1 vs session 2, $t(36) = 0.806$, $p = 0.426$, Pearson's $r = -0.162$, $p = 0.337$, **Fig. 5a**), suggesting a lack of reliability of the strength of tACS effects over time.

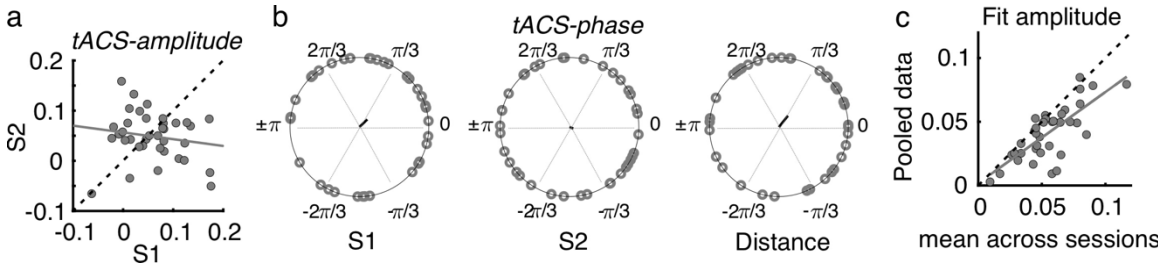

Fig 5. Effects of tACS on behavioral signatures of entrainment were not reliable over sessions. a) Amplitude of the tACS effect (*tACS-amplitude*) for session 2 as a function of session 1. *tACS-amplitude* was computed as the difference between the *FM-amplitude* values at tACS (+) and tACS (-) in **Fig. 4b**. Dashed line is the diagonal and gray solid line represents the regression line. Each dot represents a participant **b)** Optimal tACS phase lag (*tACS-phase*) estimated from the cosine fits in **(Fig. 3e)**. The first two circular plots show optimal *tACS-phase* for each session while the third one shows the circular distance between sessions. The black line is the resultant vector. **c)** The scatter plot shows the amplitude parameter obtained from fitting the cosine function to each session independently (as in **b**) and then averaged across sessions as a function of the fit amplitude obtained when fitting the cosine function to the data pooled across sessions. S1: session 1, S2: session 2.

Regarding optimal *tACS-phase,* as already mentioned in previous sections, we observed high inter-individual variability as the Rayleigh test did not indicate any significant deviation from uniformity in either session (session 1: $Z = 0.931$, $p = 0.397$; session 2: $Z = 0.133$, $p = 0.877$, **Fig. 5b**). In addition, no significant correlation between

sessions was observed (circular correlation, Rho = 0.237, p = 0.137). Moreover, the distribution of phase distances between sessions was not clustered around zero (V test with mean direction 0, V = 4.838, p = 0.130, **Fig. 5b**). Thus, contrary to the reliability we observed for the optimal *FM-phase* for gap detection, optimal *tACS-phase* lags were not stable across sessions.

We anticipated that the lack of reliability of optimal tACS phase could be influenced by a poor estimation of each single-session optimal phase lag due to a low number of trials per condition (FM-stimulus phase x Audio-tACS lag). If so, we hypothesized that the estimation of tACS effects should be strengthened by pooling data across sessions, as this would increase number of trials by a factor of 2. In this case, we expect *tACS-amplitude* to be equal or higher when estimated with the pooled data than when estimated for each separate session. However, we observed that *tACS-amplitude* was *smaller* when calculated with the pooled data than when averaging the *tACS-amplitude* across sessions (t(36) = -2.452, p = 0.019, **Fig. 5c**). We interpret the smaller *tACS-amplitude* as an indication of tACS effect cancellation due to inter-session variability. In other words, this result suggests that the lack of reliability in *tACS-phase* cannot be explained by the number of trials used for its estimation.

To better understand what factors might be influencing inter-session variability in tACS effects, we estimated multiple linear models predicting inter-session difference in *tACS-amplitude* (session 1- session 2) and absolute circular distance in *tACS-phase* between sessions from a different combinations of regressors: 1) age, 2) gender, 3) number of days passed between sessions, ΔDays, 4) absolute time of the day difference in minutes, ΔMinutes, 5) tACS-montage, and 6) inter-session difference in gap size threshold. The winning model (F-statistic vs. constant model: 5.72, p-value = 0.00735, R^2 = 0.257, **Table S2**) showed that inter-session difference in *tACS-amplitude* was significantly predicted by the number of days passed between sessions (ΔDays ß = -0.383, t = -2.55, p = 0.016) and the absolute time of the day difference (ΔMinutes ß = 0.350, t = 2.333, p = 0.026). The visualization of these effects suggested that, compared to the first session, *tACS-amplitude* decreased in session 2 for participants with longer intervals passed between sessions and for participants tested at the same time of the day (**Fig. S1**). The models predicting inter-session variability in *tACS-phase* were not significant when compared to a constant model

349 (all $p \geq 0.09$, **Table S3**). Therefore, contrary to *tACS-amplitude*, the lack of reliability in
350 *tACS-phase* cannot be explained by the interval passed between sessions or time of the day,
351 but rather may be a more fundamental feature of intra-individual variability that should
352 potentially influence the design of tACS experiments, in particular when conducted across
353 multiple sessions.

354

355 ***Inter-individual variability in the simulated E-field predicts tACS effects***

356 So far, our results demonstrate that FM-stimulus driven behavioral modulation of
357 gap detection (*FM-amplitude)* was significantly affected by the phase lag between the FM-
358 stimulus and the tACS signal (*Audio-tACS lag*). However, the strength of the tACS effect
359 was variable across participants. A natural question for us was what factors predict
360 individual variability in the magnitude of the tACS effect. Specifically, we sought to
361 explain variability in tACS effects from the seven different parameters describing the
362 optimality of the E-field simulated for each participant (**Fig. 2b**, 1) Euclidian distance
363 between the center coordinates of the functional ROI and the center coordinates of the peak
364 of the E-field, 2) spatial Pearson correlation coefficient between the individual BOLD
365 signal t-map and the electric field map, 3) mean peak E-field strength in the functional
366 ROIs, 4) peak E-field strength for the whole brain, 5) mean peak normal component of the
367 E-field for the functional ROIs, 6) peak normal component of the E-field for the whole
368 brain and 7) E-field focality); the relative strength of the BOLD signal response in the ROI
369 to the auditory stimulus; FM-driven behavioral modulation during sham stimulation; and
370 montage type (individualized vs. standard).

371 *tACS-amplitude* estimates were averaged across sessions since session did not
372 significantly affect *FM-amplitude* (**Fig. 5a**). Participants missing the fMRI session were
373 excluded and the analysis was performed with data from 34 participants (individualized
374 montage N = 16, standard montage N =18). Different linear models were fitted to the data
375 aiming to predict tACS modulation strength (averaged *tACS-amplitude*) from different
376 combinations of regressors (see Methods). The winning model (F-statistic vs. constant
377 model: 3.365, p-value = 0.017, $R^2 = 0.375$, **Fig. 6**, **Table S4**) included the main effects:
378 normal E-field (ß = -0.118, t = -0.689, p = 0.497), E-field focality (ß = 0.360, t = 1.940, p

= 0.063), average distance between the E-field peaks and the center of the target functional ROIs for each hemisphere (*Dist2Peak;* ß = -0.065, t = -0.394, p = 0.696), and the interaction terms: normal E-field: focality (ß = 0.704, t = 3.222, p = 0.003) and normal E-field:*Dist2Peak* (ß = 0.544, t = 2.799, p = 0.009*)*. Note however that only the interaction terms were significant.

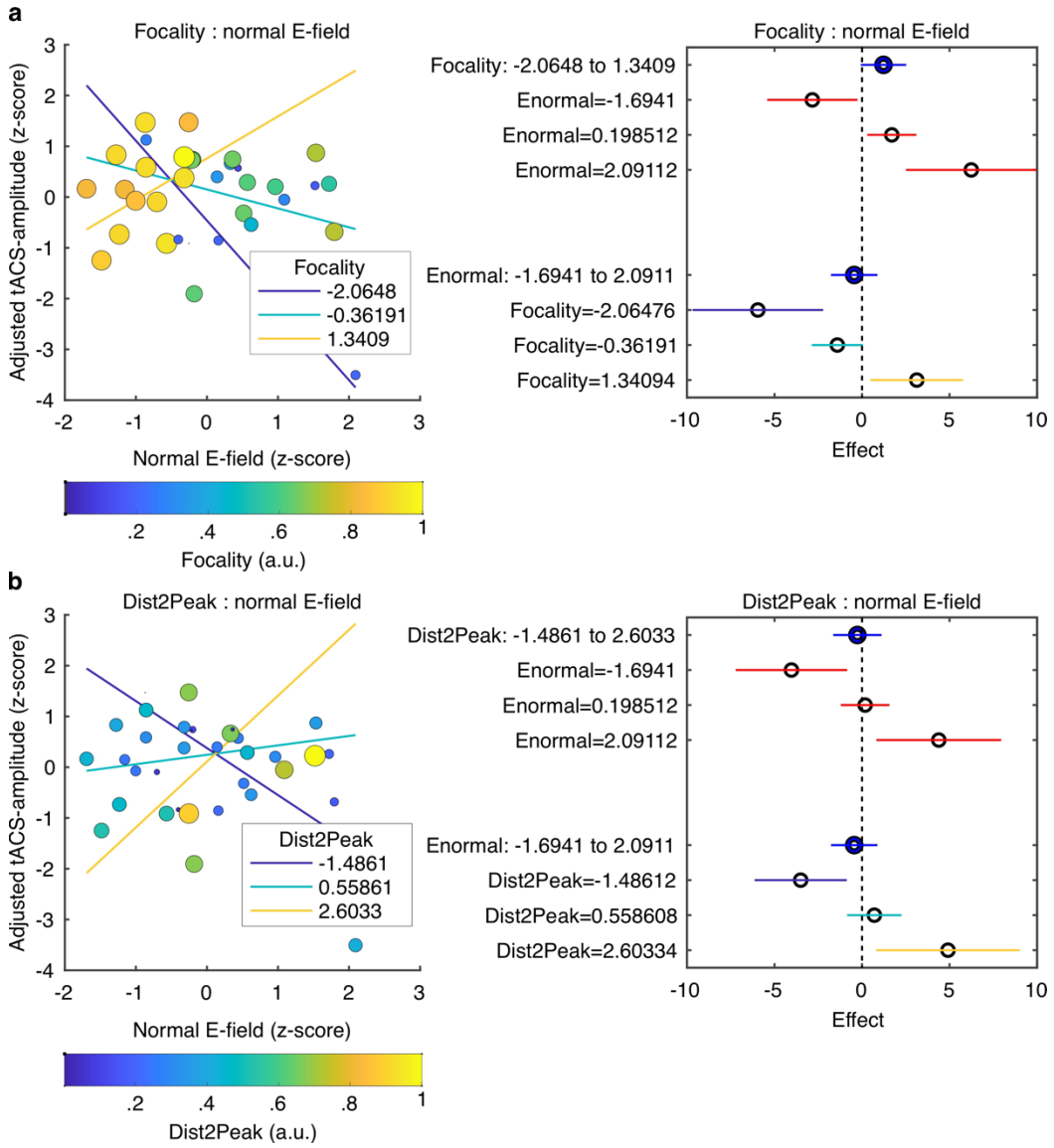

Figure 6. Predicting tACS effects from electric field simulation. a) Interaction between the normal E-field and the field focality. Scatter plot on the left shows tACS effects (*tACS-amplitude*) as a function of the normal E-field. Each dot represents a different subject. Dot color and size represent the normalized

field focality in arbitrary units. Higher values correspond to more focal electric fields. Solid lines represent the predicted adjusted response for the *tACS-amplitude* as a function of the normal E-field for three fixed values of focality. The plot in the right shows the main effects (blue) of focality and normal E-field and the conditional effect of each predictor given a specific value of the other (red). Horizontal lines through the effect values indicate their 95% confidence intervals. ***b***) Interaction between the normal E-field and the distance between the peak of the E-field and the target ROIs (*Dist2Peak*). Similar to (**a**), scatter plot on the left shows *tACS-amplitude* as a function of the normal E-field but dots color and size now represent the normalized *Dist2Peak*. Higher values correspond to shorter distance. Solid lines represent the predicted adjusted response for the *tACS-amplitude* as a function of the normal E-field for three fixed values of *Dist2Peak*. The plot in the right shows the main effects (blue) of *Dist2Peak* and normal E-field and the conditional effect of each predictor given a specific value of the other (red). Horizontal lines through the effect values indicate their 95% confidence intervals. Colors in the bottom for the Focality and *Dist2Peak* levels correspond to the same color code in the upper plots.

Visualization of the interaction terms showed that tACS effects were positively predicted by the normal E-field for participants with more focal E-fields that were closer to the functional target ROIs (**Fig. 6**). However, in participants where the induced E-field was less focal and farther from the functional target, the normal E-field negatively predicted tACS effects. The latter can be seen in the plots in **Fig 6**, where the adjusted tACS effects are shown as a function of the normal E-field at three different fixed values of focality (**Fig. 6a**) and *Dist2Peak* (**Fig. 6b**). Thus, when the electric field accurately reaches its intended target, high field strength increases behavioral consequences of tACS, but when the electric field misses its mark, high field strength is actually behaviorally detrimental.

Can we reduce inter-individual variability in tACS effects with individually optimized tACS montages?

The last question we aimed to answer was whether tACS montages individually optimized in terms of their spatial location are better for modulating auditory perception. In the previous section, the best model predicting tACS effects at the single-participant level did not include montage as a predictor, but only the normal E-field, field focality, *Dist2Peak* and their interactions. The second-best model did include montage in addition to the predictors included in the best model. However, the Akaike's information criterion corrected for small samples (AICc) from this new model was higher than the AICc of the best model by 1.294 (**Table S4**) and the likelihood ratio test suggested that the more

complex model was not better at predicting tACS effects (LRTstat = 1.917, p = 0.166). In addition, in the second-best model, the main effect of montage (ß = 0.379, t = 1.2514, p = 0.222) did not reach statistical significance. These modeling results suggest that the specific tACS montage might not have had a big impact on the size of the tACS effects overall (see Discussion). However, since testing the impact of individualizing the tACS montage was one of the main aims of the current project, we nonetheless tried to dissect the montage effects hinted at in this second-best model.

In the individualized montage group, we optimized each listener's montage by taking into account individual anatomical and functional data. One possible consequence of such approach could be a lower inter-individual variability in tACS effects, rather than an overall increase in effect size. To test this hypothesis, participants were grouped according to the electrode montage and individual *tACS-amplitude* values (see previous section) were averaged across sessions. A variance test was performed on the average *tACS-amplitude* to test whether inter-individual variability was different between montage groups. For this analysis, all participants who completed both sessions were included (individualized N = 16, standard N=21). No significant difference was observed in terms of the variance between groups ($F(20, 15) = 1.441$, $p = 0.475$).

We then took a step back and compared the group variances separated by session, and by tACS condition (tACS(+), and tACS(-), **Fig. S**2). Visual inspection of the plot suggested that inter-individual variability was smaller for the individualized montage group than for the standard montage group. To quantify this, we computed the coefficient of variation (cv) and interquartile range (iqr) for each group (session 1, individualized: tACS(+) cv = 0.3567, iqr = 0.1375, tACS(-) cv = 0.4848, iqr = 0.1480; standard: tACS(+) cv = 0.3757, iqr = 0.1684, tACS(-) cv = 0.4792, iqr = 0.1497; session 2, individualized: tACS(+) cv = 0.2531, iqr = 0.1086, tACS(-) cv = 0.2201, iqr = 0.0659; standard: tACS(+) cv = 0.3917, iqr = 0.1704, tACS(-) cv = 0.5174, iqr = 0.1736). However, the variance test was significant only for tACS(-) in session 2 (F (20,15) = 4.31, p = 0.023, *Bonferroni* corrected for 4 comparisons). No significant differences in group variance were observed for the other conditions (all F (20,15) < 1.924, p > 0.20, uncorrected). This result is suggestive, but larger sample sizes would be necessary to conduct a principled variance comparison between groups.

Discussion

In the present study, we used tACS to modulate neural entrainment to FM sounds. We tested the relevance of tACS phase lag relative to the sound rhythm and tACS montage for modulating behavioral signatures of entrainment. Our main findings show that tACS 1) does not modify the optimal FM-stimulus phase for gap detection (*FM-phase*), but 2) does modulate the amplitude of the FM-stimulus induced behavioral modulation (*FM-amplitude*) in a tACS-lag specific manner; 3) Neither the optimal tACS lag (*tACS-phase*), nor the magnitude of the phasic tACS effect (*tACS-amplitude*) were reliable across sessions; and 4) individual variability in tACS effect size was partially explained by two interactions: between the normal component of the E-field and the field focality, and between the normal component of the E-field and the distance between the peak of the electric field and the functional target ROIs. Overall, these interactions indicate that when the electric field reaches its intended target, high field strength leads to stronger behavioral effects, but when the electric field is stronger in non-target brain areas, higher field strength actually reduces the behavioral effect size.

tACS modifies the amplitude, but not the phase, of FM-stimulus induced behavioral modulation

Participants detected near-threshold silent gaps embedded in a 2 Hz FM noise stimulus. Using this paradigm, it has been repeatedly shown that EEG activity entrains to the FM rhythm and that detection of silent gaps presented in the sound is modulated by the FM-stimulus phase into which the gap falls [31-34]. Moreover, we have recently shown that both effects are reliable across participants and over time [31]. Our first hypothesis was that tACS could overwrite neural entrainment to the FM stimulus (i.e., neural oscillations phase-lock to the tACS signal instead of the FM-stimulus) and as such, the optimal FM-stimulus phase would vary as a function of tACS lag. Contrary to our prediction, results showed that in both sessions, individual optimal FM phases for gap perception were always clustered around the same phase angle, regardless of the tACS lag. We hypothesize that a reason for this could be the already strong acoustic modulation of the stimuli that we used here, which had a modulation depth of 67% peak-to-center. Phasic effects of tACS on

467 auditory perception have previously been shown mostly in the context of weakly
468 modulated background sounds [14] or for example when tACS was applied with the shape of
469 an amplitude envelope that had been acoustically removed from a speech signal [17,19]. We
470 hypothesize that entrainment to the clear rhythm of the FM stimulus might have been too
471 strong for tACS to overwrite. It has already been suggested, at least for tACS applied at
472 frequencies matching the neural alpha band, that tACS is most effective at modulating
473 oscillatory activity at the intended frequency when its power is not too high [35]. Along the
474 same line, using single unit recordings it has recently been proposed that tACS competes
475 with endogenous neural oscillations: tACS imposes its own rhythm on spiking activity
476 when tACS strength is stronger than the endogenous oscillations but it decreases rhythmic
477 spiking when tACS strength is weaker that the endogenous oscillations [36]. Thus, we would
478 predict that tACS may be more likely to shift the phase of neural entrainment when
479 entrainment is weaker to start with, either because of weaker stimulus modulation or in
480 listeners lacking young, healthy auditory systems [37].

481 Our second hypothesis was that, while tACS might not be able to overwrite
482 entrainment to a strongly modulated FM stimulus in healthy young adults, it could still
483 modulate the amplitude of the FM-driven entrainment. In other words, we anticipated that
484 tACS would interfere with neural entrainment to the FM-stimulus depending on their
485 relative phase lag: optimal tACS lag would aid neural entrainment (increase amplitude of
486 FM-driven modulation) as in constructive interference, while the opposite lag would be
487 detrimental (decrease amplitude of FM-driven modulation) since both the FM stimulus and
488 the tACS signals would try to entrain neural activity with antiphase relationships, as in
489 destructive interference. Our results showed that the amplitude of the FM-stimulus driven
490 modulation (*FM-amplitude*) was sinusoidally modulated based on the relative phase
491 between the stimulus rhythm and the electrical stimulation. Specifically, *FM-amplitude*
492 was stronger for the phase lags around the realigned optimal tACS lag and weaker for the
493 tACS lags opposite the optimal lag. Based on the association between neural entrainment
494 and auditory perception [1-8], we anticipate that making entrainment stronger with tACS
495 should lead to better cocktail party performance or better prediction/adaptation in a musical
496 context. We propose that by applying tACS at the right lag relative to auditory rhythms,
497 we can aid how the brain synchronizes to the sounds and in turn modulate behavior. Such

498 an approach might work even better when entrainment to the auditory stimulus is not
499 perfect.

500

501 ***tACS effects were not test-retest reliable***

502 The reliability of tACS effects at the individual level is not fully understood. While
503 inter-individual variability in response to electrical stimulation has been well documented
504 [24,27,28,38], most studies test tACS in only one session, and when multiple sessions are
505 conducted, a different tACS condition is implemented in each session [27,39]. Here, we tested
506 participants under the same auditory and tACS conditions in two different sessions. This
507 approach allowed us to test the stability of tACS effects across sessions. While no
508 significant difference between sessions was observed for the amplitude of tACS effects
509 (*tACS-amplitude*), tACS effects did not correlate between sessions. Moreover, no
510 significant correlation was observed between optimal tACS phase lags (*tACS-phase*) across
511 sessions, and the circular distance between sessions was not clustered. In a previous study
512 using stimuli with exactly the same parameters as in the current study, we showed neural
513 entrainment to FM-sounds has a reliable phase lag over sessions [31], so any lack of reliability
514 in optimal tACS lag cannot be explained by inconsistency on FM-stimulus-brain
515 synchrony. Our results suggest the time between sessions and the difference in time of the
516 day as possible factors influencing the inter-session variability in the strength of tACS
517 effects. However, such time factors did not explain the lack of reliability in optimal tACS-
518 phase lag.

519 The lack of test-retest reliability on tACS effects is an especially surprising result
520 from the current study which requires further investigation. The implication of this result
521 is it may not be possible to estimate optimal tACS phase lag in a session using magneto-
522 or electroencephalography and then apply it in a second session [18], but closed-loop
523 protocols where optimal tACS lag is constantly monitored during online tACS may be
524 necessary. The inconsistency of optimal tACS lags across sessions also suggests that
525 individual variability in optimal tACS lags does not arise exclusively from anatomical
526 variability but other changes in functional brain activity might be important to consider. Of
527 course, the lack of reliability could also be influenced by inconsistency in the placement of

528 the tACS electrodes across sessions, but since we took special care to precisely and
529 consistently place electrodes, we feel confident that this is a less plausible explanation.

530

531 ***tACS effects can be predicted from the simulated electric field.***

532 Several studies have already shown that inter-individual variability in tACS effects
533 can be partially explained by inter-individual variability in the strength of the simulated
534 electric field as well as the spatial overlap between this and the targeted functional area
535 [24,28,40]. Here we used a model-comparison approach to determine the parameters that best
536 explained individual variation in tACS effects; we started with E-field strength, E-field
537 focality, the correspondence between the simulated E-field and the target functional
538 regions (correlation between E-field map and BOLD map, Euclidian distance between E-
539 field and BOLD peaks), baseline factors (FM-driven modulation amplitude at sham and
540 the strength of the BOLD signal at the regions of interest) and the tACS montage. The best
541 model showed that tACS effects were best explained by the interaction between the normal
542 component of the E-field and the field focality, and the interaction between the normal E-
543 field and the distance between the E-field peak and the peak of the functional activation
544 map. The explanatory power of these interaction terms demonstrates that not only the field
545 strength is important, but also how focal it is and how optimally it targets the intended brain
546 region. For more focal electric fields targeting the correct brain regions, higher normal E-
547 fields are beneficial. However, higher normal E-fields can be detrimental when the field is
548 too broad and its peak farther away from the target ROI. This potentially relates to the fact
549 that stronger electric fields will be applied to non-relevant brain areas with unintended
550 consequences, potentially reducing the efficacy of tACS to modulate performance in the
551 target task.

552

553 ***Are individually optimized tACS montage better?***

554 In the first part of this study, we simulated Electric field strength using 3 different
555 tACS montages. The first two montages were taken from the literature [18,30] and were the
556 same for all subjects, while the third montage was individually optimized to target

individual functional ROIs using an fMRI-task localizer. Before running any simulations, we had already decided a priori to use only the individualized and standard montages for our main behavioral experiment, motivated by the fact that the 4 electrodes arrangement allows for directing the E-field in a desired orientation [30]. Directing the E-field in a desired orientation is not possible using the ring electrodes configuration from the HD montage. HD montages will always have a focus on superficial brain areas under the center electrode, and the E-field direction in the focus will be normal to the brain surface. In addition, comparing between the simulated E-fields across montages showed that the HD-montage might in fact not be optimal for modulating oscillatory activity during our specific auditory task since the peak of the induced E-field was farther from our target ROI and its strength weaker compared to the other two montages. As already described, we did not observe any difference between the individual and the group montages in terms of spatial overlap to our target ROI. While the electric field was strongest for the standard montage compared to the individualized montage, the latter induced a more focal field compared to the standard montage, therefore each montage could be good in different ways.

By using the individualized montage, we aimed to go a step past previous studies, which have shown that inter-individual variability in the E-field predicts tACS effects. Here, we asked whether tACS effects could be strengthened if the montage is optimized to each participant's anatomy and functional map, and if such approach would also reduce inter-individual variability. Compared to the standard montage, we did not observe any significant different between the overall tACS effects. We did observe a trend for decreased inter-individual variability for the individualized montage group, although this was only statistically significant for session 2 and for the amplitude of the FM-driven modulation at the non-optimal half of the tACS lags (tACS(-)).

Several points need to be considered when interpreting these results, 1) the standard montage was taken from a study where it was already optimized using anatomical and functional data from a single participant [30]. Therefore, our findings speak not to whether optimizing tACS montages is beneficial in general, but whether spatially optimizing the montage to each participant adds extra advantages. It could well be that the standard montage was already optimal for several participants with more standard brains. In fact, our individualized montage was spatially not so different from the standard one. 2) In the

current experiment, we only tested healthy young participants. We anticipate that taking into account inter-individual anatomical and functional variability will be more relevant in clinical settings or in aging research, where such variability is more evident. 3) We did not optimize the tACS protocol in terms of the applied current strength. We used a fixed value because we were limited by the size of the electrodes, and going higher than that value would make it uncomfortable for the participant. Combining spatial optimization with current-strength optimization could lead to different outcomes than what we observed here. 4) The optimization procedure here was performed with the constraints of achieving the same E-field strength in both target ROIs, inducing a relatively balanced field in both hemispheres and allowing only for 4 electrodes, i.e., two per hemisphere. Different optimization results might be obtained when optimization for more stimulation channels and allowing for a quite liberal amount of total current. Nevertheless, our results suggest that in our current settings, individualizing the tACS montage might not make a difference in terms of overall tACS effects, however it could be a way to decrease variability; given the sometimes small and highly variable nature of tACS effects in the literature, we would suggest that this may be desirable under some circumstances. However, our study was not designed to directly test the effect of tACS on sample variance, and more data would be needed to support this observation. To our knowledge, studies answering this question are missing in the tACS literature.

Conclusion

Our results showed that while tACS did not affect the optimal FM-stimulus phase for gap detection, it did modulate the amplitude of the stimulus-induced behavioral modulation, a behavioral signature of the strength of neural entrainment. Both the optimal tACS lag and the amplitude of tACS effect were variable across participants and sessions, pointing towards the potential usefulness of closed-loop stimulation protocols, where optimal lags are evaluated online during stimulation. tACS effects were predicted by the interaction between the normal component of the E-field and the field focality and the interaction between the normal E-field and the distance between the peak of the E-field and the peak of the target ROI. These results suggest that the strength of the electric field

618 is more beneficial when the E-field is closest to the target ROI and more focal, while
619 stronger normal E-field in less focal and more distant E-fields can be detrimental. While
620 no significant effect of tACS montage was observed in the overall tACS effects, the data
621 hint at lower inter-individual variability in the group with the individualized montaged
622 compared to the standard montage.

623

624 **Materials and Methods**

625 ***Participants***

626 Forty-two healthy participants took part in the study (18 females, mean age = 27.3;
627 SD = 5.8). All participants took part in at least one tACS session and 39 participants took
628 part in two tACS sessions separated by 3-301 days (median: 7 days). Data from session
629 one from one participant had to be excluded due to technical problems with the tACS signal
630 recording. From the initial sample, three individuals did not participate in the fMRI session
631 due to MRI contraindications (metal implants). All participants self-reported normal-
632 hearing and normal or corrected-to-normal vision. At the time of the experiment no
633 participant was taking medication for any neurological or psychiatric disorder.

634 Participants received financial compensation for their participation in the study.
635 Written informed consent was obtained from all participants. The procedure was approved
636 by the Ethics Council of the Max Planck Society and in accordance with the declaration of
637 Helsinki.

638

639 ***Auditory stimuli***

640 Auditory stimuli were generated by MATLAB software at a sampling rate of
641 44,100 Hz. Stimuli were 20-s long complex tones frequency modulated at a rate of 2 Hz
642 and with a center-to-peak depth of 67% of the center frequency (**Fig. 1a**). The center
643 frequency for the complex carrier signals was randomly chosen for each stimulus within
644 the range of 1000-1400Hz. The complex carrier comprised 30 components sampled from
645 a uniform distribution with a 500-Hz range. The amplitude of each component was scaled
646 linearly based on its inverse distance from the center frequency; that is, the center

frequency itself was the highest-amplitude component, and component amplitudes decreased with increasing distance from the center frequency. The onset phase of the stimulus was randomized from trial to trial, taking on one of eight values (0, π/4, π/2, 3π/4, π, 5π/4, 3π/2, 7π/4), with the constraint that each trial would always start with a phase different from its predecessor. All stimuli were rms-amplitude normalized. Each 20-s stimulus contained 3-5 silent gaps (gap onset and offset were gated with 3-ms half-cosine ramps). Each gap was chosen to be centered in 1 of 9 equally spaced phase bins into which each single cycle of the frequency modulation was divided. No gaps were presented either in the first or the last second of the stimulus. A minimum of 1.5 s separated consecutive gaps.

Procedure: Magnetic resonance imaging (MRI) session

Data acquisition. Thirty-nine participants from the initial sample took part in one session where structural and functional MRI data were collected. All images were acquired using a 3 Tesla Magnetom Prisma scanner (Siemens Healthcare, Erlangen, Germany) with a 32-channel head coil with mirror system. A three-dimensional (3D) magnetization prepared rapid gradient echo (MPRAGE) T1-weighted scan (T1w; repetition time (TR) = 2 s; echo time (TE) = 2.12 ms; flip angle (FA) = 8°; 192 sagittal slices; matrix = 256 × 256; field of view (FOV) = 256 × 256 × 192 mm3; voxel size = 1 mm^3; bandwidth = 210 Hz; selective water excitation; integrated parallel acquisition technique GRAPPA: factor 2) and a 3D turbo spin-echo (TSE) T2-weighted scan (T2w; TR = 1500 ms; TE = 356 ms; FA = 120°; 192 sagittal slices; matrix = 256 × 256; FOV = 256 × 256 × 192 mm3; voxel size = 1 mm^3; bandwidth = 331 Hz) were performed. All functional data were acquired using the 2D multiband gradient-echo echo-planar imaging sequence (EPI) with T2*-weighting (TR = 1 s, TE = 30 ms, FA = 60°, 48 slices of 2-mm thickness, 50% distance factor, in-plane resolution of 3 × 3 x 2 mm, multiband acceleration factor 4). A total of 590 whole-brain volumes were acquired in each functional run. Three functional (f)MRI runs were collected. To correct for field distortion in the functional images, a 5-volumes additional reference sequence was acquired after the first functional run with reversed phase-encoding

direction resulting in images with distortions going in opposite directions to that of the main run.

Auditory stimulation in the MRI scanner. During each functional run, participants listened to the FM stimulus and detected the silent gaps. Auditory stimuli were presented using an MR-compatible noise-cancelling headphones (OptoAcoustics OptoActive II TM ANC). These headphones reduced the EPI-gradient noise by about 20-30 dB. Prior to the main task, individual sound level and gap duration thresholds were estimated using the same procedure described for the main tACS sessions. To consider the influence of scanner noise during thresholds estimation, the same functional sequence as in the main task was run during the threshold tasks but fMRI data were not further analyzed. For the main functional runs, participants performed a version of the same task presented during the tACS sessions. Each 20-s FM-stimulus presentation was interleaved with a 20 s (+-1s) rest period during which only a fixation cross was presented in the screen. In total, participants listened to 42 FM-stimuli (14 per run) and reported the perceived gaps via a button press using a response box Current Designs Trainer 4 Buttons Inline.

Functional MRI data analysis

Preprocessing. Field distortion in the functional data was corrected using the top-up tool implemented in FSL [41]. Further data preprocessing was performed in SPM12 (7487). Preprocessing steps included: slice timing correction, motion correction, resampling to 3 × 3 × 3 mm, coregistration between structural and functional data, normalization to MNI template and 6 mm full-width-at-half-maximum-kernel Gaussian smoothing.

General linear model. Brain regions responding to the FM stimulus were identified by fitting a general linear model (GLM) to the pre-processed fMRI data for each individual participant. The model was fitted for each individual session and included tree main predictors: FM-stimulus period, detected gap periods (hits) and undetected gap periods (misses), although only the first predictor is relevant for the current analysis. Each predictor was convolved with the canonical hemodynamic response function (HRF). Time and dispersion derivatives of the HRF and a constant term were also included in the model. Additionally, the six realignment parameters were included as nuisance regressors (3 rotation (x, y, z) and 3 translation estimates (x, y, z)). For each individual, BOLD signal

706 during the FM periods was compared to the implicit baseline periods (only fixation without
707 auditory stimulation). Using the individual contrasts, a second level analysis was
708 performed to evaluate the regions responding to the FM-stimulus at the group level. A t-
709 test was performed on the group contrast and individual beta estimates were retained for
710 each participant and hemisphere, as an index of the strength of the activation.

711 ***Region of interest (ROI) definition.*** Individual T-maps for the contrast FM stimulus >
712 baseline across sessions were thresholded to p *(FWE)* < 0.001, with an extended threshold
713 of 10 voxels and masked to include only temporal regions (including the Heschl's gyrus)
714 according to the automatic anatomical labeling (AAL) atlas. For nine participants, using p
715 *(FWE)* < 0.001 for thresholding t-maps yielded either none or only unilateral activation in
716 auditory regions, therefore uncorrected $p < 0.001$ (8 participants) or $p < 0.05$ (1 participant)
717 were used instead. For each subject, FM-responsive ROI were defined by binarizing the
718 resulting t-maps. The centroid coordinates from the ROIs were estimated for each subject
719 and hemisphere. ROIs for the optimization procedure were defined by creating a 3 mm
720 radius circumference around the centroid coordinates.

721

722 **Electric field simulations and montage optimization**

723 ***Montage optimization.*** The electric field simulations and individual montage optimization
724 were implemented in SimNIBS 3.2 [42]. First, individual T1 and T2 images were segmented
725 and Finite Element Methods (FEM) head models were implemented using the headreco
726 pipeline. Small segmentation errors were corrected manually in FreeSurfer. The
727 optimization pipeline was performed in two steps. First, a lead field matrix was created per
728 individual using the 10-10 EEG virtual cap provided in SimNIBS, and the optimization
729 procedure was performed specifying two 3 mm radius spheres around the center
730 coordinates from the individual ROIs obtained from the fMRI functional localizer as the
731 target ROIs, one per hemisphere. The orientation of the E-field relative to the target ROI
732 was specified to visually resemble an auditory dipole orientation from a former study [30].
733 Four electrodes were allowed with a maximum total current of 2 mA. In a first step, the
734 algorithm was requested to optimize for a maximum electric field strength of 0.1 V/m in
735 each target, while minimizing the electric field in the eyes. The latter was done to avoid

any retinal stimulation which could induce phosphenes. Since the first optimization step did not perform as desired for all participants, because the requested E-field intensity could not be achieved at both targets, the same procedure was performed a second time but specifying the desired maximum E-field intensity to be achieved at both targets as the E-field intensity that was achieved in the first step minus 0.01 V/m. Additionally, target E-field intensity was decreased for some participants if visual inspection of the resulting E-field strength maps showed asymmetrical stimulation of the two hemispheres (10 subjects). This was done to assure obtaining a montage that would potentially stimulate both targets with the same intensity. As result, final target E-field strengths for the optimization procedure varied across participants from 0.04 – 0.09 V/m (mean: 0.071, std: 0.018).

Electric field simulations. For each participant, electric field simulations were performed for three different electrode montages: the individually optimized and two other montages previously used in the literature [18,30]. For each montage, the electric field was simulated using four electrodes, with a maximum current of 0.5 mA, to achieve a current of 1 mA peak-to-peak per channel. The specific locations for placing the electrodes for the individually optimized montage were different across participants. The HD-montage [18] included two circular electrodes of 20 mm diameter and 2 mm thickness each surrounded by a ring electrodes of 100 mm diameter and 2 mm thickness with a 75 mm diameter hole. Electrodes were placed over T7 and T8 for all participants. For the standard montage [30], electrodes were placed over FC5-TP7/P7 and FC6-TP8/P8 for all participants. For both the individualized and the standard montages, four circular electrodes were used with 25 mm diameter and 2 mm thickness, two per hemisphere. Electric field simulations were generated for each subject using the default tissue conductivities provided in SimNIBS: σ_{skin} = 0.465 S/m, σ_{skull} = 0.010 S/m, σ_{CSF} = 1.654 S/m, σ_{GM} = 0.275 S/m, σ_{WM} = 0.126 S/m, for skin, skull, cerebral spinal fluid (CSF), gray matter (GM) and white matter (WM), respectively. For each participant and montage, multiple brain maps were obtained including the strength of the electric field and its normal component and data were extracted in MATLAB using customized scripts and functions provided by SimNIBS.

Procedure: tACS sessions

The tACS sessions were conducted in an electrically shielded and acoustically isolated chamber and under normal-illumination conditions. Sound-level thresholds were determined for each participant according to the method of limits. All stimuli were then presented at 55 dB above the individual hearing threshold (55 dB sensation level, SL).

For each session, gap duration was individually adjusted to detection-threshold levels using an adaptive-tracking procedure comprising two interleaved staircases and a weighted up-down technique with custom weights as described in (Cabral-Calderin & Henry 2022). This resulted in gap durations ranging from 9-24 ms across participants and sessions (session 1: mean = 16.805 ms, SD = 3.558 ms, range = 10-24 ms; session 2: mean = 15.205, SD = 3.466, range = 9-22 ms).

Before starting the main experiment, participants performed practice trials to make sure they understood the task. For the main experiment, listeners detected gaps embedded in the 20-s long FM stimuli. Listeners were instructed to respond as quickly as possible when they detected a gap via button-press. Participants performed five blocks, each comprising the same set of 32 stimuli (4 per starting phase) but in a different randomized order. Each stimulus included 3-5 gaps for a total of 136 gaps (13-16 per phase bin, mean ~15). The number of phase bins was chosen to balance having a good sampling resolution and a high number of trials per condition without making the task too long.

Stimulation and data acquisition. Behavioral data were recorded online by MATLAB 2017a (MathWorks) in combination with Psychtoolbox. Sounds were presented at a rate of 44.1kHz, via an external soundcard (RME Fireface UCX 36-channel, USB 2.0 & FireWire 400 audio interface) using ASIO drivers. Participants listened to the sounds via over-ear headphones (Beyerdynamic DT-770 Pro 80 Ohms, Closed-back Circumaural Dynamic Diffuse field equalization Impedance: 80 Ohm SPL: 96 dB Frequency range: 5–35,000 Hz). Button presses were collected using the computer keyboard.

A battery-driven multichannel Eldith DC-stimulator Plus (NeuroConn GmbH, Ilmenau, Germany) delivered tACS through two pairs of conductive rubber electrodes

794 attached with electrode paste (Weaver and Company, Aurora, CO). Participants received
795 stimulation with one of two different electrode montages: a standard montage (applied the
796 same way to all participants) and an individualized montage (**Fig. 2a**). For the standard
797 montage, electrodes were placed over FC5-TP7/P7 and FC6-TP8/P8 as determined by the
798 International 10–20 EEG system. Note that such montage was previously optimized for
799 targeting the auditory cortex in another study [30]. For the individualized montage, electrode
800 positions could be different for each participant. Such montage was individually optimized
801 to target bilateral auditory regions of interest, determined in a functional MRI session (see
802 section: *Electric field simulations and montage optimization*; **Fig. 1f, 2a**). Each montage
803 comprised four circular electrodes with 25 mm diameter and 2 mm thickness. Each pair of
804 electrodes (one per hemisphere) was connected to a different stimulator channel. A third
805 stimulator channel using the same stimulator waveform but at lower current strength was
806 connected to an EEG amplifier (Brainamp DC amplifiers, Brain Products GmbH) in order
807 to collect the tACS signal for further analysis. The tACS signals from the additional
808 stimulator channel were collected as separate EEG channels using a split ground.

809 In each session, participants performed 5 blocks of the gap-detection task: 4 with
810 verum tACS and one with sham tACS. Verum tACS was applied at the FM-stimulus
811 frequency (2 Hz) across 4 blocks of 11 min and 20 s each for the duration of each block.
812 The current was fixed to 1 mA (peak-to-peak), and was ramped up and down over the first
813 and final 10 s of each block. Since the FM stimulus always started with a different phase,
814 and the inter-trial interval duration was jittered, the phase lag between the tACS signal and
815 the FM stimulus varied from trial to trial. Sham tACS lasted for one block of 11 min and
816 20 s, and the serial position of the sham block (out of five total) was randomized across
817 participants and also between sessions within each participant. Sham tACS was ramped on
818 over 10 s to mimic the sensation of the stimulation starting, but was then ramped back
819 down after 10 s of stimulation (ramp down 10 s for a total of 30 s stimulation). The
820 waveform of the stimulation was sinusoidal without DC offset. Impedance was kept below
821 10 kΩ.

822

823 ***Data Analysis***

824 ***Confirming behavioral entrainment in the sham condition.*** Hits were defined as gaps
825 followed by a button-press response by no earlier than 100 ms and no later than 1.5 s [31],
826 and misses were defined as gaps that were not responded to. First for the sham condition,
827 we calculated gap-detection hit rates as a function of the phase of the FM stimulus in which
828 the gaps were presented, and tested for significance of the predicted FM-induced
829 modulation of gap detection behavior. We fitted a cosine function to hit rates as a function
830 of FM phase for each participant and session. The fitted amplitude parameter (*FM-*
831 *amplitude*) quantifies the strength of the behavioral modulation by 2 Hz FM phase. The
832 optimal FM phase (*FM-phase*) is the phase that yields peak predicted gap-detection hit
833 rate. The intercept parameter corresponds to mean hit rate across FM phases, and was not
834 analyzed further here. Significance of the behavioral modulation (*FM-amplitude*) was
835 tested using a permutation approach, whereby 1000 surrogate datasets were created for
836 each participant and session by shuffling the single-gap accuracy values (0,1) with respect
837 to their FM-stimulus phase bin labels. Cosine functions were also fitted to the surrogate
838 datasets. Gap detection was considered to be significantly modulated for each participant
839 if the individual FM-amp value was higher than the 95th percentile of the distribution of
840 FM-amp values from the surrogate data, corresponding to $p < 0.05$).

841 ***Evaluating tACS effects.*** In order to determine the tACS phase timecourse for each trial in
842 the verum stimulation blocks, the tACS signal collected in the EEG was band-pass filtered
843 between 1-10 Hz, submitted to a Hilbert transform, and the complex output was converted
844 to phase angles (4-quadrant inverse tangent, *atan2*). For each gap, the phase lag between
845 the 2-Hz FM stimulus and the 2-Hz tACS signal was estimated as the circular distance
846 between their instantaneous phases at the 2-Hz FM stimulus onset. Individual gaps were
847 then sorted into 6 FM–tACS phase-lags bins centered on 0, $\pi/3$, $2\pi/3$, π, $-2\pi/3$, and $-\pi/3$
848 (see **Fig. 3a**). Hit rates were calculated separately for each of the 9 FM-phase bins and the
849 6 FM–tACS lags (plus the sham condition, as described above). Cosine fits were used to
850 estimate *FM-amplitude* and *FM-phase* for each participant, session, and FM–tACS lag.

851 The effect of FM–tACS lag on FM-phase was evaluated by investigating whether
852 *FM-phase* were clustered around the same value for all tACS conditions using the V-test

853 as implemented in the circular statistic toolbox [43]. To estimate the effect of FM–tACS lag
854 on *FM-amplitude*, a second-level cosine function was fitted to the *FM-amplitude* values as
855 a function of FM–tACS lag. From this second-level fit, the optimal tACS phase lag (*tACS-*
856 *phase*) was defined as the FM–tACS lag yielding the highest predicted *FM-amplitude*
857 value.

858 ***Evaluating tACS effects at the group level.*** *TACS-phase* values were highly variable
859 across individuals. Thus, in order to fairly evaluate FM–tACS effects on *FM-amplitude* at
860 the group level, FM-amplitude values were circularly realigned so that optimal tACS-phase
861 was zero-phase for each participant and session. To control for possible analytical biases
862 induced by the alignment procedure, *FM-amplitude* at the individual optimal tACS lag and
863 *FM-amplitude* at the opposite phase were excluded from further analysis (Riecke et al.,
864 2015). We statistically tested mean *FM-amplitude* values for positive against negative
865 realigned phase values: *FM-amplitude* values for positive FM–tACS lags (tACS(+)) were
866 *FM-amplitude* averaged across the two tACS lags adjacent to the aligned zero-lag
867 condition, and *FM-amplitude* values for negative FM–tACS lags (tACS(-)) were *FM-*
868 *amplitude* averaged across the two tACS lags adjacent to the tACS lag opposite the
869 realigned zero-lag condition. Group tACS effects were then assessed using a repeated
870 measures (rm)ANOVA with the factors tACS lag condition (3 levels: sham, tACS(+), and
871 tACS(-)) and session (2 levels: S1 and S2) as the repeated measures.

872

873 ***Evaluating the reliability of tACS effects.***

874 Reliability of the strength of tACS effects was investigated by comparing *tACS-*
875 *amplitude* values between sessions as well as via Pearson's correlation coefficient.
876 Reliability of *tACS-phase* was assessed by computing the circular distance between *tACS-*
877 *phase* across sessions and testing its distribution against zero. In addition, circular-to-
878 circular correlation of tACS-phase across sessions was employed.

879

880 ***Predicting tACS effects with linear models.*** The difference between FM-amplitude at the
881 positive half of the tACS cycle (tACS(+)) and the FM-amplitude at the negative half of the

882 tACS cycle (tACS(-)) was first calculated for each subject and session and then averaged
883 across sessions. This average difference was taken as the overall tACS effect (*tACS-*
884 *amplitude*) for each participant. We aimed to test the influence of the electric field
885 characteristics and baseline performance (i.e., *FM-amplitude* at sham, auditory-driven
886 BOLD signal increase) on tACS effects. To do this, we fit several linear models using the
887 MATLAB function '*fitlm*'. Each model evaluated whether inter-individual variability in
888 tACS effects could be predicted as a function of seven parameters extracted from the
889 simulated electric field: 1) mean Euclidian distance between the center coordinates of the
890 functional ROIs (one per hemisphere) and the center coordinates of the peak of the electric
891 field in each hemisphere (where the peak is for the 99-percentile-thresholded E-field
892 strength across all voxels for the given hemisphere), 2) spatial Pearson correlation
893 coefficient between the individual BOLD signal t-map and the electric field map, 3) peak
894 E-field strength for the whole brain (based on the 95-percentile-thresholded E-field map),
895 4) mean peak E-field strength in the functional ROIs (based on the 95-percentile-
896 thresholded E-field from a 7 mm sphere around the center coordinates of the functional
897 ROIs), 5) peak normal component of the E-field for the whole brain (95-percentile-
898 thresholded), 6) peak normal component of the E-field in the functional ROIs (defined as
899 in 4) and 7) E-field focality (cortical area in mm^2 with E-field strength higher than the 50th
900 percentile). Additional regressors in the model included baseline predictors: 8) amplitude
901 of the FM-induced behavioral modulation at sham, averaged over sessions, 9) mean beta
902 estimates from the BOLD signal map; and the 10) tACS montage (individualized vs
903 standard montage); and the interaction between the terms. All predictors were transformed
904 to z-scores prior to model fitting. Before z-score transformation, the field focality and the
905 *Dist2Peak* predictors were inverted so higher values mean higher focality and shorter
906 distance. Thirty-three different models were fitted, each including a different combination
907 of regressors, and the best model was selected using the Akaike's information criterion
908 corrected for small samples (AICc, **Table S4**) and the Likelihood Ratio Test (LRT).

909 Additional linear models were estimated using the same procedure as describe
910 above but to evaluate the effect of regressors 1) gender, 2) age 3) number of days between
911 sessions, ΔDays, 4) inter-session time on the day difference in minutes, ΔMinutes, 5) inter-
912 session difference in gap size threshold and 6) montage on the inter-session reliability of

913 tACS effects: inter-session difference in *tACS-amplitude* (session 1- session 2) and
914 absolute circular distance in tACS-phase. For each dependent variable, multiple models
915 were tested (**Tables S2-3**). Significance and model selection were performed as above.

916

917 ***Evaluating the effect of the electrode montage on inter-individual variability.***

918 A variance test was performed on the *tACS-amplitude* values averaged across
919 sessions and grouped by tACS montage to test for the effect of montage on inter-subject
920 variability in the overall tACS effect. Additional variance tests were performed on the *FM-*
921 *amplitude* values for tACS(+) and tACS(-) separated by session to check for montage-
922 specific differences in inter-individual variability specific to a given tACS condition and
923 session. Resultant p-values were corrected for 4 comparisons using the Bonferroni method.
924 For descriptive information on inter-individual variability for each group and condition,
925 the coefficient of variation (CV) and the interquartile ratio (iqr) were calculated.

926

927 ***Other Statistical Analyses***

928 Unless otherwise specified, correlation analyses between linear variables were done
929 using Pearson correlation coefficient. In case of circular data, circular–circular or circular–
930 linear correlations were computed using the respective functions in the circular statistics
931 toolbox for MATLAB [43]. Different between tACS montages in terms of the simulated
932 electric fields were investigated using rmANOVAs. Post-hoc analyses were conducted
933 using standard paired t-tests. Significant p-values were corrected using *Bonferroni* method.

934 Data and Matlab codes will be made publicly available in
935 https://edmond.mpdl.mpg.de/dataset.xhtml?persistentId=doi%3A10.17617%2F3.0W1CN
936 C&version=DRAFT after publication.

References

1 Peelle, J. E. & Davis, M. H. Neural Oscillations Carry Speech Rhythm through to Comprehension. *Front Psychol* **3**, 320 (2012). https://doi.org:10.3389/fpsyg.2012.00320

2 Golumbic, E. M. Z. *et al.* Mechanisms Underlying Selective Neuronal Tracking of Attended Speech at a "Cocktail Party". *Neuron* **77**, 980-991 (2013). https://doi.org:10.1016/j.neuron.2012.12.037

3 Horton, C., D'Zmura, M. & Srinivasan, R. Suppression of competing speech through entrainment of cortical oscillations. *J Neurophysiol* **109**, 3082-3093 (2013). https://doi.org:10.1152/jn.01026.2012

4 Doelling, K. B., Arnal, L. H., Ghitza, O. & Poeppel, D. Acoustic landmarks drive delta-theta oscillations to enable speech comprehension by facilitating perceptual parsing. *Neuroimage* **85 Pt 2**, 761-768 (2014). https://doi.org:10.1016/j.neuroimage.2013.06.035

5 Horton, C., Srinivasan, R. & D'Zmura, M. Envelope responses in single-trial EEG indicate attended speaker in a 'cocktail party'. *J Neural Eng* **11**, 046015 (2014). https://doi.org:10.1088/1741-2560/11/4/046015

6 Doelling, K. B. & Poeppel, D. Cortical entrainment to music and its modulation by expertise. *Proc Natl Acad Sci U S A* **112**, E6233-6242 (2015). https://doi.org:10.1073/pnas.1508431112

7 Nozaradan, S., Peretz, I. & Keller, P. E. Individual Differences in Rhythmic Cortical Entrainment Correlate with Predictive Behavior in Sensorimotor Synchronization. *Sci Rep* **6**, 20612 (2016). https://doi.org:10.1038/srep20612

8 Brodbeck, C., Jiao, A., Hong, L. E. & Simon, J. Z. Neural speech restoration at the cocktail party: Auditory cortex recovers masked speech of both attended and ignored speakers. *PLoS Biol* **18**, e3000883 (2020). https://doi.org:10.1371/journal.pbio.3000883

9 Herrmann, C. S., Rach, S., Neuling, T. & Struber, D. Transcranial alternating current stimulation: a review of the underlying mechanisms and modulation of cognitive processes. *Front Hum Neurosci* **7**, 279 (2013). https://doi.org:10.3389/fnhum.2013.00279

10 Reato, D., Rahman, A., Bikson, M. & Parra, L. C. Effects of weak transcranial alternating current stimulation on brain activity-a review of known mechanisms from animal studies. *Front Hum Neurosci* **7**, 687 (2013). https://doi.org:10.3389/fnhum.2013.00687

11 Cabral-Calderin, Y. & Wilke, M. Probing the Link Between Perception and Oscillations: Lessons from Transcranial Alternating Current Stimulation. *Neuroscientist* **26**, 57-73 (2020). https://doi.org:10.1177/1073858419828646

12 Krause, M. R., Vieira, P. G., Csorba, B. A., Pilly, P. K. & Pack, C. C. Transcranial alternating current stimulation entrains single-neuron activity in the primate brain.

Proc Natl Acad Sci U S A **116**, 5747-5755 (2019). https://doi.org:10.1073/pnas.1815958116

13 Johnson, L. *et al.* Dose-dependent effects of transcranial alternating current stimulation on spike timing in awake nonhuman primates. *Sci Adv* **6** (2020). https://doi.org:10.1126/sciadv.aaz2747

14 Riecke, L., Sack, A. T. & Schroeder, C. E. Endogenous Delta/Theta Sound-Brain Phase Entrainment Accelerates the Buildup of Auditory Streaming. *Curr Biol* **25**, 3196-3201 (2015). https://doi.org:10.1016/j.cub.2015.10.045

15 Riecke, L., Formisano, E., Sorger, B., Baskent, D. & Gaudrain, E. Neural Entrainment to Speech Modulates Speech Intelligibility. *Curr Biol* **28**, 161-169 e165 (2018). https://doi.org:10.1016/j.cub.2017.11.033

16 Wilsch, A., Neuling, T., Obleser, J. & Herrmann, C. S. Transcranial alternating current stimulation with speech envelopes modulates speech comprehension. *Neuroimage* **172**, 766-774 (2018). https://doi.org:10.1016/j.neuroimage.2018.01.038

17 Zoefel, B., Archer-Boyd, A. & Davis, M. H. Phase Entrainment of Brain Oscillations Causally Modulates Neural Responses to Intelligible Speech. *Curr Biol* **28**, 401-408 e405 (2018). https://doi.org:10.1016/j.cub.2017.11.071

18 van Bree, S., Sohoglu, E., Davis, M. H. & Zoefel, B. Sustained neural rhythms reveal endogenous oscillations supporting speech perception. *PLoS Biol* **19**, e3001142 (2021). https://doi.org:10.1371/journal.pbio.3001142

19 Zoefel, B., Allard, I., Anil, M. & Davis, M. H. Perception of Rhythmic Speech Is Modulated by Focal Bilateral Transcranial Alternating Current Stimulation. *J Cogn Neurosci* **32**, 226-240 (2020). https://doi.org:10.1162/jocn_a_01490

20 Preisig, B. C. *et al.* Selective modulation of interhemispheric connectivity by transcranial alternating current stimulation influences binaural integration. *Proc Natl Acad Sci U S A* **118** (2021). https://doi.org:10.1073/pnas.2015488118

21 Keshavarzi, M., Varano, E. & Reichenbach, T. Cortical Tracking of a Background Speaker Modulates the Comprehension of a Foreground Speech Signal. *J Neurosci* **41**, 5093-5101 (2021). https://doi.org:10.1523/JNEUROSCI.3200-20.2021

22 Erkens, J., Schulte, M., Vormann, M. & Herrmann, C. S. Lacking Effects of Envelope Transcranial Alternating Current Stimulation Indicate the Need to Revise Envelope Transcranial Alternating Current Stimulation Methods. *Neurosci Insights* **15**, 2633105520936623 (2020). https://doi.org:10.1177/2633105520936623

23 Coldea, A., Morand, S., Veniero, D., Harvey, M. & Thut, G. Parietal alpha tACS shows inconsistent effects on visuospatial attention. *PLoS One* **16**, e0255424 (2021). https://doi.org:10.1371/journal.pone.0255424

24 Kasten, F. H., Duecker, K., Maack, M. C., Meiser, A. & Herrmann, C. S. Integrating electric field modeling and neuroimaging to explain inter-individual variability of tACS effects. *Nat Commun* **10**, 5427 (2019). https://doi.org:10.1038/s41467-019-13417-6

25 Cabral-Calderin, Y. *et al.* Transcranial alternating current stimulation affects the BOLD signal in a frequency and task-dependent manner. *Hum Brain Mapp* **37**, 94-121 (2016). https://doi.org:10.1002/hbm.23016

26 Evans, C. *et al.* Dose-controlled tDCS reduces electric field intensity variability at a cortical target site. *Brain Stimul* **13**, 125-136 (2020). https://doi.org:10.1016/j.brs.2019.10.004

27 Cabral-Calderin, Y., Williams, K. A., Opitz, A., Dechent, P. & Wilke, M. Transcranial alternating current stimulation modulates spontaneous low frequency fluctuations as measured with fMRI. *Neuroimage* **141**, 88-107 (2016). https://doi.org:10.1016/j.neuroimage.2016.07.005

28 Zanto, T. P. *et al.* Individual differences in neuroanatomy and neurophysiology predict effects of transcranial alternating current stimulation. *Brain Stimul* **14**, 1317-1329 (2021). https://doi.org:10.1016/j.brs.2021.08.017

29 Stecher, H. I. & Herrmann, C. S. Absence of Alpha-tACS Aftereffects in Darkness Reveals Importance of Taking Derivations of Stimulation Frequency and Individual Alpha Variability Into Account. *Front Psychol* **9**, 984 (2018). https://doi.org:10.3389/fpsyg.2018.00984

30 Baltus, A., Wagner, S., Wolters, C. H. & Herrmann, C. S. Optimized auditory transcranial alternating current stimulation improves individual auditory temporal resolution. *Brain Stimul* **11**, 118-124 (2018). https://doi.org:10.1016/j.brs.2017.10.008

31 Cabral-Calderin, Y. & Henry, M. J. Reliability of Neural Entrainment in the Human Auditory System. *J Neurosci* **42**, 894-908 (2022). https://doi.org:10.1523/JNEUROSCI.0514-21.2021

32 Henry, M. J. & Obleser, J. Frequency modulation entrains slow neural oscillations and optimizes human listening behavior. *Proc Natl Acad Sci U S A* **109**, 20095-20100 (2012). https://doi.org:10.1073/pnas.1213390109

33 Henry, M. J., Herrmann, B. & Obleser, J. Entrained neural oscillations in multiple frequency bands comodulate behavior. *Proc Natl Acad Sci U S A* **111**, 14935-14940 (2014). https://doi.org:10.1073/pnas.1408741111

34 Bauer, A. R., Bleichner, M. G., Jaeger, M., Thorne, J. D. & Debener, S. Dynamic phase alignment of ongoing auditory cortex oscillations. *Neuroimage* **167**, 396-407 (2018). https://doi.org:10.1016/j.neuroimage.2017.11.037

35 Neuling, T., Rach, S. & Herrmann, C. S. Orchestrating neuronal networks: sustained after-effects of transcranial alternating current stimulation depend upon brain states. *Front Hum Neurosci* **7**, 161 (2013). https://doi.org:10.3389/fnhum.2013.00161

36 Krause, M. R., Vieira, P. G., Thivierge, J. P. & Pack, C. C. Brain stimulation competes with ongoing oscillations for control of spike timing in the primate brain. *PLoS Biol* **20**, e3001650 (2022). https://doi.org:10.1371/journal.pbio.3001650

37 Rufener, K. S., Oechslin, M. S., Zaehle, T. & Meyer, M. Transcranial Alternating Current Stimulation (tACS) differentially modulates speech perception in young and older adults. *Brain Stimul* **9**, 560-565 (2016). https://doi.org:10.1016/j.brs.2016.04.002

38 Li, L. M., Uehara, K. & Hanakawa, T. The contribution of interindividual factors to variability of response in transcranial direct current stimulation studies. *Front Cell Neurosci* **9**, 181 (2015). https://doi.org:10.3389/fncel.2015.00181

39 Antal, A. *et al.* Comparatively weak after-effects of transcranial alternating current stimulation (tACS) on cortical excitability in humans. *Brain Stimul* **1**, 97-105 (2008). https://doi.org:10.1016/j.brs.2007.10.001

40 Preisig, B. C. & Hervais-Adelman, A. The Predictive Value of Individual Electric Field Modeling for Transcranial Alternating Current Stimulation Induced Brain Modulation. *Front Cell Neurosci* **16**, 818703 (2022). https://doi.org:10.3389/fncel.2022.818703

41 Smith, S. M. *et al.* Advances in functional and structural MR image analysis and implementation as FSL. *Neuroimage* **23 Suppl 1**, S208-219 (2004). https://doi.org:10.1016/j.neuroimage.2004.07.051

42 Saturnino, G. B., Siebner, H. R., Thielscher, A. & Madsen, K. H. Accessibility of cortical regions to focal TES: Dependence on spatial position, safety, and practical constraints. *Neuroimage* **203**, 116183 (2019). https://doi.org:10.1016/j.neuroimage.2019.116183

43 Berens, P. CircStat: A MATLAB Toolbox for Circular Statistics. *J Stat Softw* **31**, 1-21 (2009). https://doi.org:DOI 10.18637/jss.v031.i10